Discovery of the type-II superconductor $Ta_4Rh_2C_{1-\delta}$ with a high upper critical field

KeYuan Ma [1], Sara López-Paz,[2] Karolina Gornicka,[3,2] Harald O. Jeschke [4], Tomasz Klimczuk,[3] and Fabian O. von Rohr [2,*]

[1]*Max Planck Institute for Chemical Physics of Solids, 01187 Dresden, Germany*

[2]*Department of Quantum Matter Physics, University of Geneva, CH-1211 Geneva, Switzerland*

[3]*Faculty of Applied Physics and Mathematics and Advanced Materials Centre, Gdansk University of Technology, Gdansk 80-233, Poland*

[4]*Research Institute for Interdisciplinary Science, Okayama University, Okayama 700-8530, Japan*

(Received 16 October 2024; accepted 11 April 2025; published 14 May 2025)

We report on the discovery of superconductivity in the previously unknown compound $Ta_4Rh_2C_{1-\delta}$. $Ta_4Rh_2C_{1-\delta}$ crystallizes in the η-carbide structure type, in the cubic space group $Fd\bar{3}m$ (No. 227) with a unit cell parameter of $a = 11.7947$ Å. Temperature-dependent magnetic susceptibility, resistivity, and specific-heat capacity measurements reveal that $Ta_4Rh_2C_{1-\delta}$ is a type-II bulk superconductor with a critical temperature of $T_c = 6.4$ K and a normalized specific-heat jump $\Delta C/\gamma T_c = 1.56$. Notably, we find that $Ta_4Rh_2C_{1-\delta}$ has a high upper critical field of $\mu_0 H_{c2}(0) = 17.4$ T, which exceeds the BCS weak-coupling Pauli limit of $\mu_0 H_{\text{Pauli}} = 11.9$ T.

DOI: 10.1103/PhysRevResearch.7.023147

I. INTRODUCTION

The discovery of new superconductors with enhanced properties for diverse applications remains a significant challenge in condensed matter physics [1–4]. A crucial property for these applications is the upper critical field $\mu_0 H_{c2}(0)$, which is essential for technological applications [5]. When an external magnetic field is applied to a superconductor, Cooper pairs may break due to two effects: the orbital-limiting effect, which induces a momentum leading to a supercurrent that exceeds the superconducting gap, and the Pauli paramagnetic effect (Zeeman effect), where the Zeeman energy surpasses the superconducting condensation energy [6]. Near the critical temperature T_c, the orbital-limiting effect dominates, while the Pauli paramagnetic effect is more significant at lower temperatures. In BCS theory, the maximum $\mu_0 H_{c2}(0)$ is limited by the Pauli paramagnetic effect, known as the Pauli paramagnetic limit $\mu_0 H_{\text{Pauli}}$, given as $\mu_0 H_{\text{Pauli}} \approx 1.86\,[\text{T/K}] \times T_c$ [6]. Several superconductors with the η-carbide-type crystal structure have recently been found to violate the Pauli paramagnetic limit, exhibiting very high upper critical fields [7–9].

The η-carbide-type compounds crystallize in the cubic space group $Fd\bar{3}m$, and commonly form with compositions of A_4B_2X and A_3B_3X, where A and B stand for transition metals, and X for carbon, nitrogen, or oxygen [10–13]. The η-carbide-type compounds consist of more than 100 known members with combinations of different technologically useful properties such as high hardness, high thermal stability, rich variety of magnetic states, exotic electronic properties, and catalytic properties [14–16]. One of the most striking characteristics of η-carbide compounds is that they exist over wide ranges of chemical compositions and allow for a high degree of atomic substitutions [17]. In this structure type, tuning of the chemical composition allows for modifying and controlling of the physical properties in a wide range. Hence, the flexibility and tunability of the η-carbide structure provide numerous opportunities to achieve new quantum materials with intriguing physical properties.

Among the systematically investigated η-carbide-type superconductors, Ti_4Co_2O, Ti_4Ir_2O, $Nb_4Rh_2C_{1-\delta}$, and Zr_4Pd_2O were found to have $\mu_0 H_{c2}(0)$ larger than the weak-coupling Pauli limit, where $\mu_0 H_{\text{Pauli}} \approx 1.86\,[\text{T/K}] \times T_c$ [7–9,18]. These isostructural superconductors share many electronic property features; therefore, it is likely they also share a common origin for the unusually high upper critical fields. Recently, in the high-field region of Ti_4Ir_2O, signatures for a Fulde-Ferrell-Larkin-Ovchinnikov state have been observed and μSR measurements have revealed a small superfluid density in the superconducting state of Ti_4Ir_2O [19]. Both observations point towards unconventional superconductivity in this family of materials. Therefore, the η-carbide family of compounds has become a fertile ground for the discovery of novel superconducting materials.

Here, we report on the discovery of superconductivity in the previously unknown η-carbide compound $Ta_4Rh_2C_{1-\delta}$. We find $Ta_4Rh_2C_{1-\delta}$ to crystallize in the η-carbide structure type with a unit cell parameter of $a = 11.7947$ Å. Furthermore, we show that this compound is a type-II bulk superconductor with a critical temperature of $T_c = 6.4$ K and a specific-heat jump $\Delta C/\gamma T_c$ of 1.56. Moreover, we find that $Ta_4Rh_2C_{1-\delta}$—like some other η-carbide superconductors—has a very high upper critical field of $\mu_0 H_{c2}(0)$ of 17.4 T, which exceeds the weak-coupling Pauli paramagnetic limit $\mu_0 H_{\text{Pauli}}$ of 11.9 T.

II. EXPERIMENTAL DETAILS

Synthesis. Polycrystalline $Ta_4Rh_2C_{1-\delta}$ was synthesized from nearly stoichiometric amounts of the elements using

*Contact author: fabian.vonrohr@unige.ch

tantalum powder (99.99%, Alfa Aesar), rhodium powder (99.95%, Strem Chemicals), and carbon rod (99.999%, Sigma-Aldrich). A total mass of 150 mg of starting material was used. The reactants were thoroughly mixed in an agate mortar and pressed into a pellet. The pellet was first melted in an arc furnace in a purified argon atmosphere on a water-cooled copper plate. The sample was flipped over and molten five times to ensure an optimal homogeneity. After arc melting, only a small mass loss of approximately 1% was observed. The very hard solidified melt ingot was crushed into small particles in a tungsten carbide mortar and ground to fine powders in an agate mortar and pressed into a pellet. The pellet was wrapped with thin Ta foil, sealed in a quartz tube under a 1/3 atm argon, and annealed in a furnace for 4 days at 1200 °C. After reaction, the quartz tube was cooled down to room temperature by quenching in water.

Structure and composition. The crystal structure and phase purity of the sample were checked using powder x-ray diffraction (PXRD) measurements on a Rigaku SmartLab diffractometer with Cu K_α radiation in Bragg-Brentano reflection geometry. The PXRD patterns were collected in the 2Θ range of 5–120° with a scan rate of 0.25°/min. Rietveld refinements were performed using the FULLPROF program package [20]. The chemical composition of the polycrystalline samples was examined under a scanning electron microscope (SEM) (JEOL JSM-IT800 operated at 15 keV) equipped with an energy-dispersive x-ray (EDX) spectrometer.

Physical property measurements. Temperature- and field-dependent magnetization measurements were performed on a Quantum Design magnetic properties measurement system (MPMS3) with a 7 T magnet equipped with a vibrating sample magnetometry (VSM) option. The measured pellet was placed parallel to the external magnetic field to minimize the demagnetization effects in the superconducting state. The electrical resistivity and specific-heat capacity measurements were conducted in a Quantum Design physical property measurement system (PPMS) with a 9 T magnet. For the resistivity measurements, the four-probe technique was employed with gold wires connected to the sample with silver paint. Specific-heat measurements were performed with the Quantum Design heat-capacity option, using a relaxation technique.

Electronic structure calculations. We performed density functional theory (DFT) calculations based on the full potential local orbital (FPLO) basis set [21] to understand the electronic structure of $Ta_4Rh_2C_{1-\delta}$. Due to heavy elements Ta and to some extent Rh, spin-orbit coupling is expected to be strong in $Ta_4Rh_2C_{1-\delta}$, and we use fully relativistic calculations with the generalized gradient approximation exchange-correlation functional [22] to account for the spin-orbit-coupling effects in the electronic structure. We converge the calculations on $16 \times 16 \times 16$ k meshes.

III. RESULTS AND DISCUSSION

A. Synthesis

Here, we report the η-carbide compound $Ta_4Rh_2C_{1-\delta}$ in the ternary Ta-Rh-C phase-space system. We have obtained polycrystalline $Ta_4Rh_2C_{1-\delta}$ as a silver-colored pellet. Achieving a phase-pure $Ta_4Rh_2C_{1-\delta}$ sample proved to be challenging. Direct high-temperature reactions of mechanically mixed elements pressed into a pellet produced low-quality samples with multiple phases. This is likely due to the difficulty in homogeneously mixing the grains of the reactants. We found that arc melting the reactants was crucial, even though the η-carbide phase was not present in the ingot immediately after arc melting, but seems to allow for optimal mixing of the elements (see Supplemental Material, Fig. S1 [23]). In preparative chemistry, the synthesis of phase-pure ternary η-carbides is generally known to be challenging [11,24]. In a series of synthesis experiments, the highest-purity final samples were obtained with a starting ratio of Ta:Rh:C as 3.85:2.15:0.85. Deviation from this compositional ratio or from the annealing temperature (1200 °C) resulted in the formation of significant impurity phases.

TABLE I. Atomic and cell parameters of $Ta_4Rh_2C_{1-\delta}$ obtained from Rietveld refinement of the room-temperature PXRD data.

Atom	Site	x	y	z	B_{iso}	Occ.
Ta1	16*c*	0	0	0	1.13(1)	1
Rh	32*e*	0.21185(7)	0.21185(7)	0.21185(7)	0.77(3)	1
Ta2	48*f*	0.44067(7)	0.125	0.125	1.13(1)	1
C	16*d*	0.5	0.5	0.5	1.1*	1
$Fd\bar{3}m$ (no. 227); $a = 11.7947(1)$ Å						
R_p (%) = 5.97: R_{wp} (%) = 9.56; R_{Bragg} (%) = 5.43						

Note: Here, $*B_{iso}$ is fixed to the refined overall value.

B. Crystal structure

We find $Ta_4Rh_2C_{1-\delta}$ to crystallize in the η-carbide-type structure, with the cubic space group $Fd\bar{3}m$ (no.227) with the cell parameter of $a = 11.7947(1)$ Å. This structure can be rationalized as related compounds, e.g., $Nb_4Rh_2C_{1-\delta}$ [$a = 11.8527(2)$ Å] also crystallize in it. Here, the powder x-ray diffraction technique was employed to identify the phase purity and cell parameters of the obtained samples.

The powder x-ray diffraction (PXRD) pattern and the corresponding Rietveld refinement of the obtained $Ta_4Rh_2C_{1-\delta}$ sample are presented in Fig. 1(a). Energy-dispersive x-ray spectroscopy (EDS) analysis reveals a Ta:Rh ratio of 1.9(5):1 for the sample, which is close to the ideally stoichiometric value of 2:1. Reliable quantification of the carbon content by EDS is not possible and is challenging by x-ray diffraction as well (see Supplemental Material [23]). Assuming only a negligible carbon loss during the arc-melting process, the carbon content in $Ta_4Rh_2C_{1-\delta}$ should be close to 0.85, i.e., the nominal composition, for the amount of carbon used for the purest obtained sample. Rietveld refinement analysis determined that the main phase, $Ta_4Rh_2C_{1-\delta}$, constitutes 96.5% of the sample, with a minor impurity phase of Ta_2O_5 at 3.5%. Notably, the formation of TaC as an impurity phase was not observed for these synthesis conditions. Details on the Rietveld refinements of Ta_4Rh_2C are summarized in Table I, assuming a model η-carbide structure type, with the cubic space group $Fd\bar{3}m$ and Ta_4Rh_2C stoichiometry.

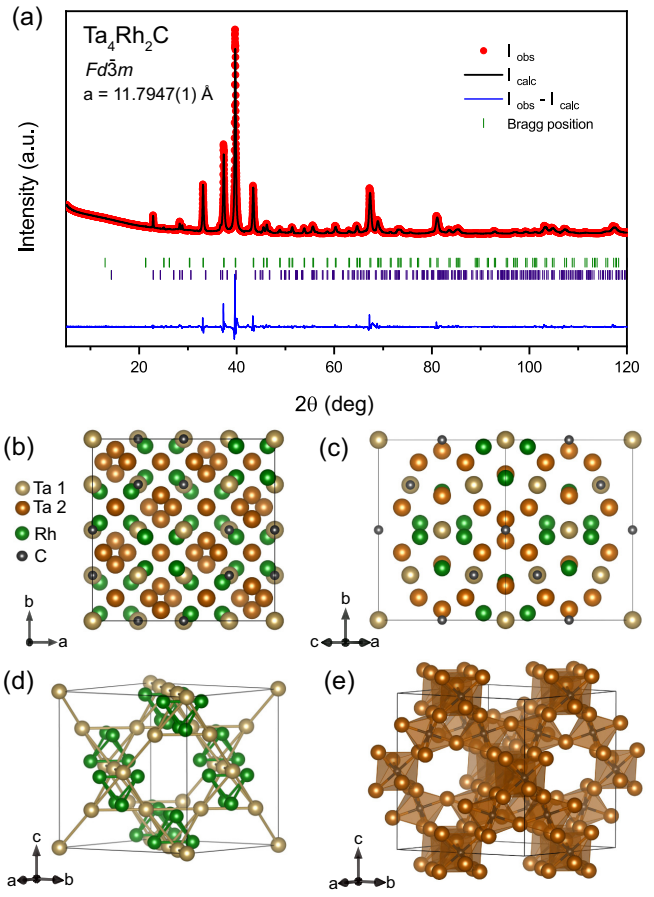

FIG. 1. (a) Rietveld refinements of the room-temperature PXRD pattern of $Ta_4Rh_2C_{1-\delta}$. The plots are represented as follows: observed (red dots), calculated (black line), and difference (blue line) intensities. The Bragg positions of the main $Ta_4Rh_2C_{1-\delta}$ phase [96.5(4)%] and Ta_2O_5 impurity phase [3.5(1)%] are indicated with green and purple vertical ticks, respectively. (b)–(e) Schematic representation of different orientations for the refined crystal structure from PXRD of $Ta_4Rh_2C_{1-\delta}$.

In Figs. 1(b)–1(e), we show the crystal structure of $Ta_4Rh_2C_{1-\delta}$ in an ideal chemical stoichiometric general formula of Ta_4Rh_2C. In this η-carbide structure, Ta atoms occupy the 16*c* and the 48*f* Wyckoff positions, Rh atoms occupy the 32*e* Wyckoff positions, and C atoms occupy the 16*d* Wyckoff positions. Even though there are only four Wyckoff positions required to describe the crystal structure, the unit nevertheless contains results in a total of 112 atoms and a formula of $Ta_{64}Rh_{32}C_{16}$ for one unit cell. In Figs. 1(b) and 1(c), the unit cell with all atoms is shown in two orientations. In Fig. 1(d), the connectivity of the Ta1 and Rh atoms is shown: the Ta1 atoms form a network of tetrahedra resulting in a stella quadrangla structure, while the Rh atoms arrange in isolated tetrahedra. The Ta2 atoms form a network of octahedra in which every second one is slightly distorted, as shown in Fig. 1(e), with the C atoms filling the octahedral voids.

C. Physical properties

To understand the physical properties of the η-carbide compound $Ta_4Rh_2C_{1-\delta}$, we performed temperature-dependent magnetic susceptibility, resistivity, and specific-heat capacity measurements.

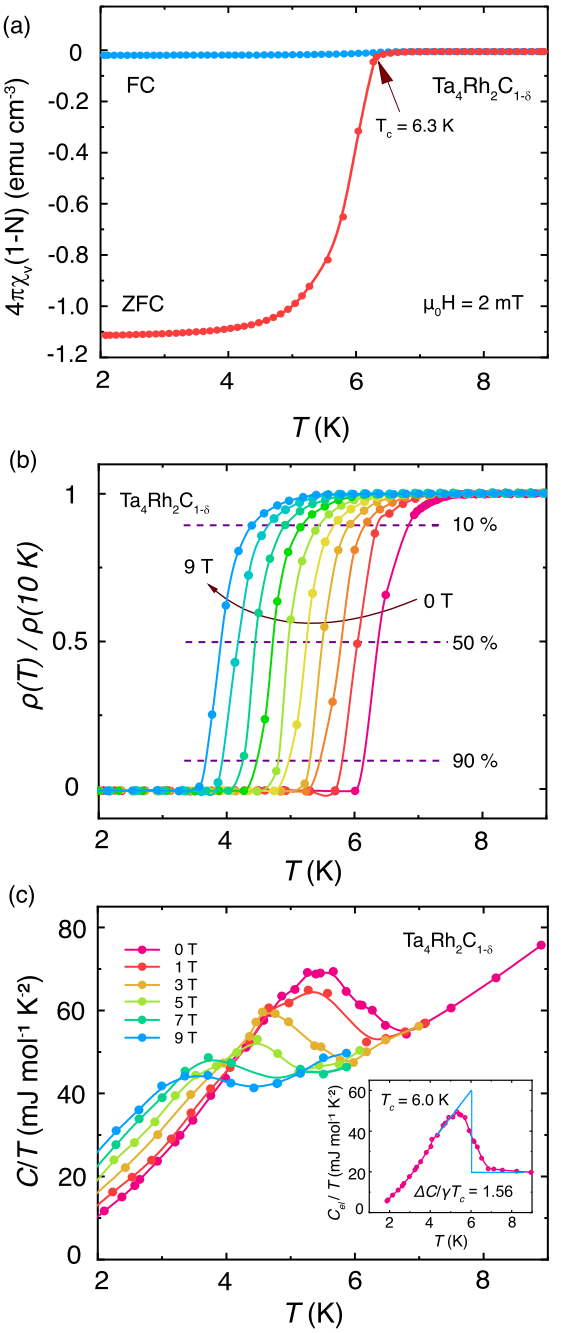

FIG. 2. Superconducting properties of $Ta_4Rh_2C_{1-\delta}$. (a) Zero-field-cooled (ZFC) and field-cooled (FC) temperature-dependent magnetic susceptibility in a temperature range from $T = 2$ to 9 K. (b) Field-dependent resistivity in the vicinity of the superconducting transition in fields between $\mu_0 H = 0$ and 9 T. (c) Field-dependent specific heat in fields between $\mu_0 H = 0$ and 9 T. Inset: Entropy-conserving construction of the zero-field measurement.

In Fig. 2(a), we observe a superconducting transition at a critical temperature of $T_c = 6.3$ K in the temperature dependence of the magnetic susceptibility in zero-field-cooled (ZFC) and field-cooled (FC) modes under an external field

of $\mu_0 H = 2\,\mathrm{mT}$, respectively. The difference between the FC and ZFC measurements in the superconducting state is characteristic of a type-II superconductor. When dealing with the magnetic susceptibility data, a demagnetization factor N was estimated using the relationship $-b = 1/[4\pi(1-N)]$ [25]. Here, we obtain a value of $N = 0.53$ for our sample by fitting the field-dependent measurements of the magnetization to a line ($M = bH + a$) in the low-field region [25].

In the normal state, $Ta_4Rh_2C_{1-\delta}$ shows a Pauli paramagnetic behavior, as confirmed by the magnetization measurement between 10 and 300 K in an external field of $\mu_0 H = 1\,\mathrm{T}$ (see Supplemental Material, Fig. S3 [23]). To estimate the lower critical field H_{c1}, we performed a series of field-dependent measurements of the magnetization in low fields below the critical temperature T_c, as shown in Fig. S4(a) of the Supplemental Material [23]. Here, we used the magnetic-field point where the $M(H)$ curve first deviates from linearity as the measure for H_{c1} [26]. With this approximation, the obtained H_{c1} values are fitted using the semiempirical formula

$$H_{c1}(T) = H_{c1}(0)[1 - (T/T_c)^2]. \tag{1}$$

The lower critical field at $T = 0\,\mathrm{K}$ is determined to be $\mu_0 H_{c1}(0) = 9.4\,\mathrm{mT}$, as shown in Fig. S4(b) of the Supplemental Material [23]. After taking the demagnetization factor $N = 0.53$ into account, the lower critical field is corrected to be $\mu_0 H^*_{c1}(0) = 20\,\mathrm{mT}$.

We find the resistivity of $Ta_4Rh_2C_{1-\delta}$ to decrease with decreasing temperature, showing a metallic behavior. The temperature-dependent electrical resistivity measurement of the polycrystalline $Ta_4Rh_2C_{1-\delta}$ sample from 300 to 1.8 K is shown in the Supplemental Material (see Fig. S5 [23]). At a critical temperature $T_{c,\mathrm{onset}}$ of 7.2 K, $Ta_4Rh_2C_{1-\delta}$ starts to undergo a transition to a superconducting state and the resistivity completely drops to zero at 6.0 K. Here, the residual resistivity ratio (RRR) value of the annealed polycrystalline sample is defined as $\rho(300\,\mathrm{K})/\rho(10\,\mathrm{K}) \approx 1.22$, corresponding to a poor metal behavior. This small RRR value may arise from the polycrystalline nature of the sample. In Fig. 2(b), we show the temperature- and field-dependent resistivity $\rho(T, H)$ in a temperature range from $T = 2$ to 9 K and magnetic fields between $\mu_0 H = 0$ and 9 T. We show that the resistivity drops to zero at the transition to the superconducting state for all applied fields. In zero field, we determine the critical temperature to be $T_c = 6.4\,\mathrm{K}$ with a 50% criterion. As expected, the critical temperature decreases steadily as the applied magnetic field increases. However, the critical temperature is only suppressed to $T_c = 3.9\,\mathrm{K}$ in the maximal applied field of 9 T, which is already evidence of the remarkably high upper critical field of this superconductor.

In Fig. 2(c), we present the temperature- and field-dependent specific heat $C(T, H)$ in the vicinity of the superconducting transitions, where the data are plotted as C/T versus T in magnetic fields between $\mu_0 H = 0$ and 9 T. The specific-heat jumps corresponding to the superconducting transitions are well pronounced in all measured fields, and shift to lower temperatures, which are in good agreement with the results from the resistivity measurements. At zero field, the specific-heat jump temperature corresponding to the superconducting transition is determined to be $T_c = 6.0\,\mathrm{K}$ based on an entropy-conserving construction, as shown in the inset of Fig. 2(c).

In the normal state—close to the superconducting transition—the specific heat can be fitted according to the expression

$$\frac{C(T)}{T} = \frac{C_{el} + C_{ph}}{T} = \gamma + \beta T^2, \tag{2}$$

where γ is the Sommerfeld coefficient, corresponding to the electronic contribution to $C(T)$, and βT^3 is the phonon contribution to the specific heat. Here, we obtain the γ to be 20.9 mJ mol^{-1} K^{-2}, and the β to be 0.707 mJ mol^{-1} K^{-4} for $Ta_4Rh_2C_{1-\delta}$ (see Supplemental Material, Fig. S6 [23]). With the above obtained T_c and γ values, the normalized specific-heat jump is found to be $\Delta C/\gamma T_c = 1.56$ in zero field, which is slightly larger than the weak-coupling BCS value of 1.43 and evidence for the bulk nature of the superconducting state in $Ta_4Rh_2C_{1-\delta}$.

We determined the Debye temperature to be $\Theta_D = 268\,\mathrm{K}$, using the following relationship:

$$\Theta_D = \left(\frac{12\pi^4}{5\beta} nR\right)^{\frac{1}{3}}. \tag{3}$$

Here, $n = 7$ is the number of atoms per formula unit, and $R = 8.314$ J mol^{-1} K^{-1} is the ideal gas constant.

The electron-phonon coupling constant λ_{ep} can be estimated from the Debye temperature, using the semiempirical McMillan approximation [27],

$$\lambda_{ep} = \frac{1.04 + \mu^* \ln\left(\frac{\Theta_D}{1.45T_c}\right)}{(1 - 0.62\mu^*)\ln\left(\frac{\Theta_D}{1.45T_c}\right) - 1.04}. \tag{4}$$

Here, the Coulomb repulsion parameter μ^* is set to be 0.13 according to an empirical approximation that was widely used in superconductors with similar elements (e.g., $NbRh_2B_2$ and $TaRh_2B_2$) [25,28–31]. Based on these values, the λ_{ep} value for $Ta_4Rh_2C_{1-\delta}$ is calculated to be 0.71, which is smaller than the value 0.83 for $Nb_4Rh_2C_{1-\delta}$.

The measured γ value corresponds to a density of states at the Fermi level of $D(E_F)$ of 5.23 states eV^{-1} per formula unit (f.u.) in $Ta_4Rh_2C_{1-\delta}$, when using the following relationship:

$$D(E_F) = \frac{3\gamma}{\pi^2 k_B^2 (1 + \lambda_{ep})}. \tag{5}$$

D. High upper critical field in $Ta_4Rh_2C_{1-\delta}$

In Fig. 3(a), we present the field dependence of the critical temperatures T_c determined from the resistivity measurements using the common 10%, 50%, and 90% criteria, as well as the specific-heat capacity as shown in Figs. 2(b) and 2(c) (compare, e.g., Refs. [7,28,32]). When using the Ginzburg-Landau (GL) formalism, the zero-temperature upper critical field $\mu_0 H_{c2}(0)$ for $Ta_4Rh_2C_{1-\delta}$ is determined to be 23.5, 20.7, 20.1, and 21.3 T for the 10%, 50%, and 90% criteria of resistivity and the specific-heat capacity, respectively (see Supplemental Material, Fig. S7 [23]). Usually, a Ginzburg-Landau (GL) model fitting will give higher estimated upper critical field values for the η-carbide structure-type superconductors [7,8,19].

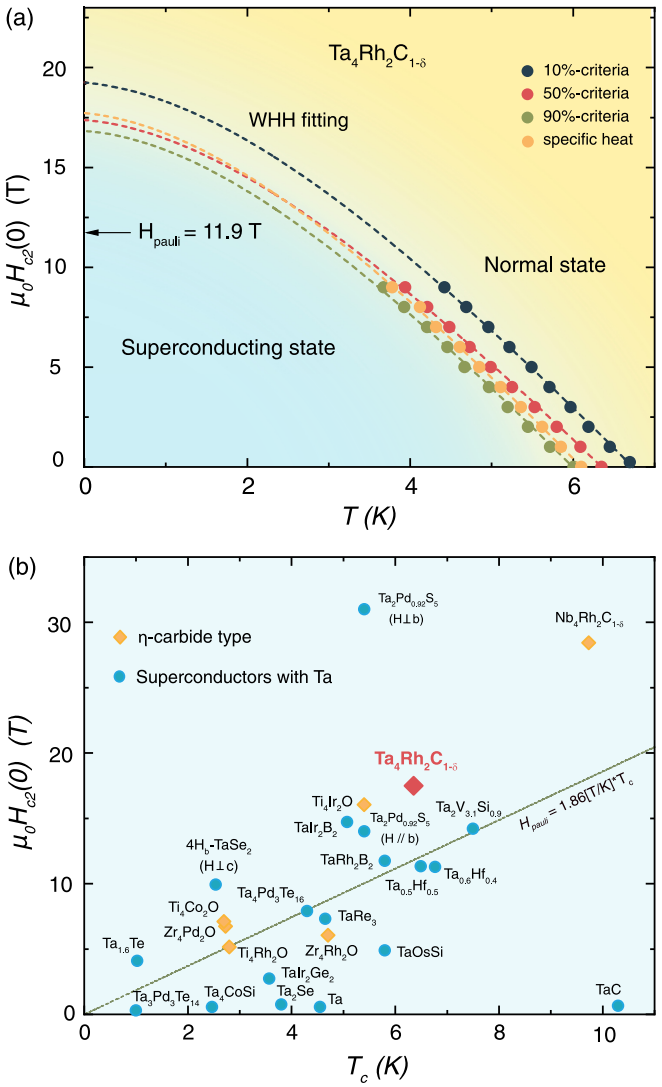

FIG. 3. (a) Upper critical field $\mu_0 H_{c2}$ of $Ta_4Rh_2C_{1-\delta}$. Data points from field- and temperature-dependent resistivity using the 10%, 50%, 90% criteria, and specific-heat capacity measurements are shown. The data points were fitted using Eq. (6). The presented weak-coupling BCS Pauli limit $H_{\rm Pauli} \approx 1.86\,[{\rm T/K}] \times T_c$ was calculated using T_c values from the 50% criterion of resistivity. (b) Comparison of $Ta_4Rh_2C_{1-\delta}$ in T_c and $\mu_0 H_{c2}(0)$ with previously reported η-carbide-type superconductors and superconductors containing Ta.

Here, we make a conservative estimation of the upper critical field $\mu_0 H_{c2}(0)$ for $Ta_4Rh_2C_{1-\delta}$ using the Werthamer-Helfand-Hohenberg (WHH) formalism in the dirty limit according to [7,33,34],

$$\mu_0 H_{c2}(T) = \frac{\mu_0 H_{c2}(0)}{0.693} h^*_{\rm fit}(t), \tag{6}$$

with $h^*_{\rm fit}$ being

$$h^*_{\rm fit}(t) = (1-t) - C_1(1-t)^2 - C_2(1-t)^4, \tag{7}$$

where $t = T/T_c$ (T_c is the transition temperature at zero field), while $C_1 = 0.153$ and $C_2 = 0.152$ are two parameters [34]. The zero-temperature upper critical field $\mu_0 H_{c2}(0)$ is determined to be 19.3, 17.4, 16.9, and 17.7 T for the 10%, 50%, and 90% criteria of resistivity and the specific-heat capacity, respectively. All of these values exceed the corresponding weak-coupling BCS Pauli paramagnetic limits of $\mu_0 H_{\rm Pauli} \approx 1.86\,[{\rm T/K}] \times T_c = 12.5$, 11.9, 11.1, and 11.2 T, respectively.

In Fig. 3(b), we present a comparison of $Ta_4Rh_2C_{1-\delta}$ with previously reported superconductors containing Ta in T_c and $\mu_0 H_{c2}(0)$ evaluation [25,29,31,35–46]. The critical temperature T_c of $Ta_4Rh_2C_{1-\delta}$ is higher than most of the reported Ta-based superconductors and its $\mu_0 H_{c2}(0)$ value is higher than all the listed known superconductors, except the highly anisotropic $Ta_2Pd_{0.92}S_6$, when this material is measured with the applied field vertical to the b axis [43]. Until now, reported Ta-based superconductors with a $\mu_0 H_{c2}(0)$ value higher than the weak-coupling Pauli limit have been limited to $TaRh_2B_2$, $TaIr_2B_2$, $Ta_2Pd_{0.92}S_6$, $4H_b - TaSe_2$, $Ta_2V_{3.1}Si_{0.9}$, and the quasicrystal superconductor $Ta_{1.6}Te$ [25,29,43–46]. All these superconductors have highly anisotropic crystal structures. In contrast to this, the crystal structure of $Ta_4Rh_2C_{1-\delta}$ is cubic and centrosymmetric, which strongly reflects the unusual nature of the Pauli limit violation in this material. It should be noted that $Ta_4Rh_2C_{1-\delta}$ has the second-highest critical temperature T_c and upper critical field $\mu_0 H_{c2}(0)$ values among all reported η-carbide structure-type superconductors, to date [7–9,47].

E. Parameters in the superconducting state of $Ta_4Rh_2C_{1-\delta}$

The obtained upper critical field $\mu_0 H_{c2}(0)$ value, together with the lower critical field $\mu_0 H^*_{c1}(0)$ value, can be used to calculate other relevant superconducting parameters for $Ta_4Rh_2C_{1-\delta}$. Here, the $\mu_0 H_{c2}(0)$ value from the 50% criterion is 17.4 T and it corresponds to a superconducting Ginzburg-Landau coherence length of $\xi_{\rm GL} = 43.5$ Å according to the following equation:

$$\mu_0 H_{c2}(0) = \frac{\Phi_0}{2\pi\,\xi^2_{\rm GL}}, \tag{8}$$

where $\Phi_0 = h/(2e) \approx 2.0678 \times 10^{-15}$ Wb is the quantum flux. The superconducting penetration depth $\lambda_{\rm GL}$ can be estimated from the values of $\xi_{\rm GL}$ and $\mu_0 H^*_{c1}$ obtained above by using the relation

$$\mu_0 H^*_{c1} = \frac{\Phi_0}{4\pi\lambda^2_{\rm GL}} \ln\left(\frac{\lambda_{\rm GL}}{\xi_{\rm GL}}\right). \tag{9}$$

We obtained a value of $\lambda_{\rm GL} = 1743$ Å for $Ta_4Rh_2C_{1-\delta}$. The value of $\kappa_{\rm GL} = \lambda_{\rm GL}/\xi_{\rm GL}$ is calculated to be 40. These values demonstrate that $Ta_4Rh_2C_{1-\delta}$ is a type-II superconductor with a short superconducting coherence length $\xi_{\rm GL}$ and a large superconducting penetration depth $\lambda_{\rm GL}$.

In Table II, we list all the parameters that we have obtained for $Ta_4Rh_2C_{1-\delta}$ and compare them with the isostructural superconductor $Nb_4Rh_2C_{1-\delta}$. We find that the superconducting properties of $Ta_4Rh_2C_{1-\delta}$ are similar to those of $Nb_4Rh_2C_{1-\delta}$, especially the high upper critical field exceeding the weak-coupling Pauli limit. Therefore, $Ta_4Rh_2C_{1-\delta}$ is both isostructural and isoelectronic to its sister compound $Nb_4Rh_2C_{1-\delta}$. Previously, the isostructural and isoelectronic Nb/Ta superconducting sister compounds pairs NbC-TaC [39], $NbRh_2B_2 - TaRh_2B_2$ [25], and $NbIr_2B_2 - TaIr_2B_2$ [29] have been explored and compared. Here, $Ta_4Rh_2C_{1-\delta}$ and

TABLE II. Summary of all the determined parameters of $Ta_4Rh_2C_{1-\delta}$ and the comparison with $Nb_4Rh_2C_{1-\delta}$.

Parameters	Units	$Ta_4Rh_2C_{1-\delta}$	$Nb_4Rh_2C_{1-\delta}$
$T_{c,m}$	K	6.3	9.7
$T_{c,r}$	K	6.4	9.8
$T_{c,h}$	K	6.0	9.5
RRR		1.22	1.16
$\mu_0 H^*_{c1}(0)$	mT	20	13.6
$\mu_0 H_{c2}(0)$	T	17.4	28.5
β	mJ mol^{-1} K^{-4}	0.7	0.6
γ	mJ mol^{-1} K^{-2}	21	40
λ_{ep}		0.71	0.83
Θ_D	K	268	283
ξ_{GL}	Å	44	34
λ_{GL}	Å	1743	2252
κ_{GL}		40	66.2
$\Delta C/\gamma T_c$		1.56	1.64
$D_{exp}(E_F)$	states eV^{-1}/f.u.	5.23	9.32
$D_{cal}(E_F)$	states eV^{-1}/f.u.	5.45	9.63
$\mu_0 H_{c2}(0)/T_c$	T/K	2.85	2.92

Note: The $\mu_0 H^*_{c1}(0)$ value for $Ta_4Rh_2C_{1-\delta}$ is corrected with a demagnetization factor.

$Nb_4Rh_2C_{1-\delta}$ represent a different pair of isostructural and isoelectronic Nb/Ta superconducting compounds.

F. Electronic structure of $Ta_4Rh_2C_{1-\delta}$

We performed density functional theory calculations for $Ta_4Rh_2C_{1-\delta}$ based on the structure determined in this work and given in Table I. Figure 4 shows the band structure and density of states (DOS) of $Ta_4Rh_2C_{1-\delta}$. We perform the calculation for $\delta = 0$, but we determine the amount of hole doping that a carbon deficiency of $\delta = 0.15$ would entail; it is marked by a pink region in Fig. 4. As Ta is chemically similar to Nb, it is not surprising that the electronic structure of $Ta_4Rh_2C_{1-\delta}$ does resemble the electronic structure of $Nb_4Rh_2C_{1-\delta}$ (see Ref. [7]). From the calculated DOS shown in Fig. 4(b), the DOS at E_F with $\delta = 0.15$ gives a theoretical value of 5.45 states eV^{-1}/f.u., which is comparable with the value of 5.23 states eV^{-1}/f.u. calculated from the heat-capacity measurement (see Table II). Similarly, in the previous study on $Nb_4Rh_2C_{1-\delta}$, the DOS at E_F with $\delta = 0.3$ provided a theoretical value of 9.63 states eV^{-1}/f.u., which is close to the experimentally derived value of 9.32 states eV^{-1}/f.u. from the heat-capacity measurement (see Ref. [7]).

We have also compared the effect of spin-orbit coupling on the band structures of Nb_4Rh_2C and Ta_4Rh_2C, respectively. We find significantly stronger splitting of bands in Ta_4Rh_2C, indicating stronger effects of spin-orbit coupling due to the replacement of the 5*d* transition metal Ta for the 4*d* transition metal Nb (see Supplemental Material, Fig. S8 [23]). In the Supplemental Material [Figs. S9 and S10], we present the calculated Fermi surface of $Nb_4Rh_2C_{1-\delta}$ with $\delta = 0$, and $\delta = 0.15$, respectively [23].

IV. CONCLUSION

In summary, we have successfully synthesized a new η-carbide superconductor $Ta_4Rh_2C_{1-\delta}$ by arc melting, followed by the high-temperature annealing method. Our x-ray diffraction measurements show that $Ta_4Rh_2C_{1-\delta}$ crystallizes in the η-carbide structure type, and is isostructural to the known superconductor $Nb_4Rh_2C_{1-\delta}$. Our systematic temperature-dependent magnetic susceptibility, resistivity, and specific-heat capacity measurements show that $Ta_4Rh_2C_{1-\delta}$ is a bulk superconductor with a critical temperature of T_c of 6.4 K, and a specific-heat jump value $\Delta C/\gamma T_c$ of 1.56, close to the weak-coupling BCS value of 1.43.

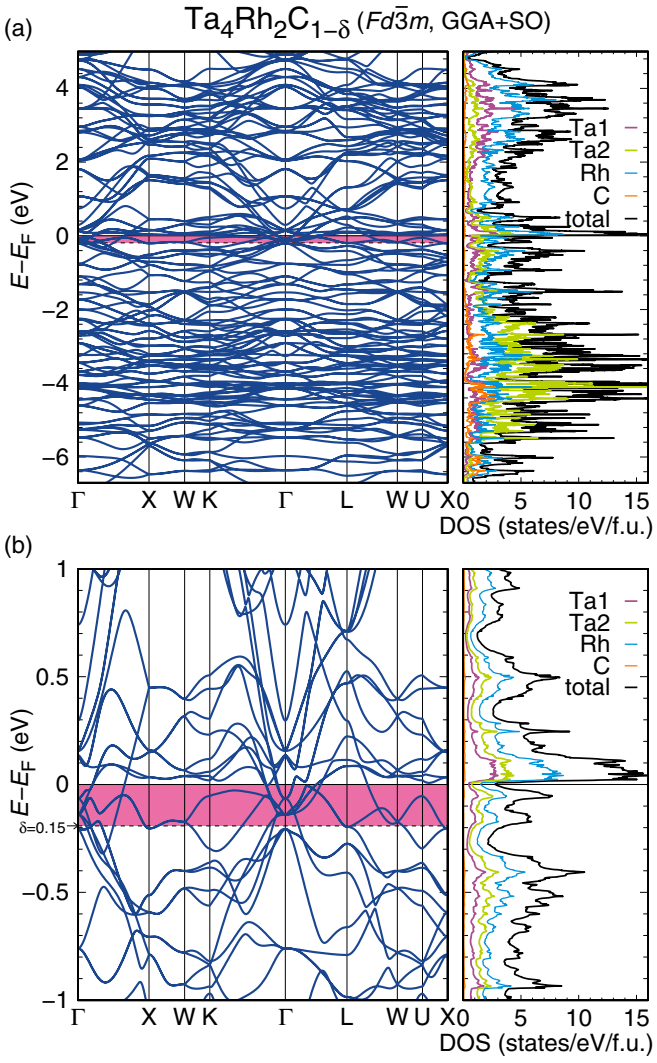

FIG. 4. Electronic structure of $Ta_4Rh_2C_{1-\delta}$ calculated with GGA + SO. (a) Overview and (b) detail of the band structure and density of states. Pink shading indicates the range $0 \leqslant \delta \leqslant 0.15$.

It is indeed an extreme type-II superconductor with a $\kappa_{GL} = \lambda_{GL}/\xi_{GL}$ of 40. The upper critical field $\mu_0 H_{c2}(0)$ of 17.4 T exceeds the weak-coupling BCS Pauli paramagnetic limit of $\mu_0 H_{Pauli} = 11.9$ T. All these intriguing properties make $Ta_4Rh_2C_{1-\delta}$ an exotic superconductor similar to its sister compound $Nb_4Rh_2C_{1-\delta}$. In the future, the development of improved preparation techniques to obtain single-phase or even single-crystal samples of these η-carbide-type superconductors for the development of superconducting wires, but also for an improved understanding of the underlying superconducting mechanism, is highly desired.

ACKNOWLEDGMENTS

This work was supported by the Swiss National Science Foundation under Grant No. PCEFP2_194183. Research performed at Gdansk University of Technology was supported by the National Science Center (Poland), Project No. 2022/45/B/ST5/03916.

[1] D. Larbalestier and P. C. Canfield, Superconductivity at 100—Where we've been and where we're going, MRS Bull. **36**, 590 (2011).

[2] F. O. von Rohr, Chemical principles of intrinsic topological superconductors, Chem. Mater. **35**, 9455 (2023).

[3] A. Simon, Superconductivity and chemistry, Angew. Chem. Intl. Ed. **36**, 1788 (1997).

[4] A. Santoro, F. Beech, M. Marezio, and R. Cava, Crystal chemistry of superconductors: A guide to the tailoring of new compounds, Physica C: Superconductivity **156**, 693 (1988).

[5] S. Hahn, K. Kim, K. Kim, X. Hu, T. Painter, I. Dixon, S. Kim, K. R. Bhattarai, S. Noguchi, J. Jaroszynski *et al.*, 45.5-tesla direct-current magnetic field generated with a high-temperature superconducting magnet, Nature (London) **570**, 496 (2019).

[6] M. Tinkham, *Introduction to Superconductivity* (McGraw-Hill, New York, 1996).

[7] K. Ma, K. Gornicka, R. Lefèvre, Y. Yang, H. M. Rønnow, H. O. Jeschke, T. Klimczuk, and F. O. von Rohr, Superconductivity with high upper critical field in the cubic centrosymmetric η-carbide $Nb_4Rh_2C_{1-\delta}$, ACS Mater. Au **1**, 55 (2021).

[8] K. Ma, R. Lefèvre, K. Gornicka, H. O. Jeschke, X. Zhang, Z. Guguchia, T. Klimczuk, and F. O. von Rohr, Group-9 transition-metal suboxides adopting the filled-Ti_2Ni structure: A class of superconductors exhibiting exceptionally high upper critical fields, Chem. Mater. **33**, 8722 (2021).

[9] Y. Watanabe, A. Miura, C. Moriyoshi, A. Yamashita, and Y. Mizuguchi, Observation of superconductivity and enhanced upper critical field of η-carbide-type oxide Zr_4Pd_2O, Sci. Rep. **13**, 22458 (2023).

[10] K. Kuo, The formation of η carbides, Acta Metall. **1**, 301 (1953).

[11] H. Ku and D. Johnston, New superconducting ternary transition metal compounds with the $E9_3$-type structure, Chin. J. Phys. **22**, 59 (1984).

[12] S. Gupta, D. J. Sordelet, and J. D. Corbett, Structural and compositional investigations of Zr_4Pt_2O: A filled-cubic Ti_2Ni-type phase, J. Solid State Chem. **182**, 1708 (2009).

[13] R. Mackay, G. J. Miller, and H. F. Franzen, New oxides of the filled-Ti_2Ni type structure, J. Alloys Compd. **204**, 109 (1994).

[14] T. Waki, Y. Umemoto, S. Terazawa, Y. Tabata, A. Kondo, K. Sato, K. Kindo, S. Alconchel, F. Sapina, Y. Takahashi *et al.*, Itinerant electron metamagnetism in η-carbide-type compound Co_3Mo_3C, J. Phys. Soc. Jpn. **79**, 093703 (2010).

[15] T. J. Prior and P. D. Battle, Superparamagnetism and metal-site ordering in quaternary nitrides with the η-carbide structure, J. Mater. Chem. **14**, 3001 (2004).

[16] S. Cui, A. C. Mtukula, X. Bo, and L. Guo, High-efficiency Co_6W_6C catalyst with three-dimensional ginger-like morphology for promoting the hydrogen and oxygen evolution reactions, Intl. J. Hydrogen Energy **45**, 6404 (2020).

[17] A. Taylor and K. Sachs, A new complex eta-carbide, Nature (London) **169**, 411 (1952).

[18] B.-B. Ruan, M.-H. Zhou, Q.-S. Yang, Y.-D. Gu, M.-W. Ma, G.-F. Chen, and Z.-A. Ren, Superconductivity with a violation of Pauli limit and evidences for multigap in η-carbide type Ti_4Ir_2O, Chin. Phys. Lett. **39**, 027401 (2022).

[19] D. Das, K. Y. Ma, J. Jaroszynski, V. Sazgari, T. Klimczuk, F. O. von Rohr, and Z. Guguchia, Ti_4Ir_2O: A time reversal invariant fully gapped unconventional superconductor, Phys. Rev. B **110**, 174507 (2024).

[20] J. Rodriguez-Cavajal, Recent developments of the program FULLPROF, Comm. Powder Diffract. Newsl. **26**, 12 (2001).

[21] K. Koepernik and H. Eschrig, Full-potential nonorthogonal local-orbital minimum-basis band-structure scheme, Phys. Rev. B **59**, 1743 (1999).

[22] J. P. Perdew, K. Burke, and M. Ernzerhof, Generalized gradient approximation made simple, Phys. Rev. Lett. **77**, 3865 (1996).

[23] See Supplemental Material at http://link.aps.org/supplemental/10.1103/PhysRevResearch.7.023147 for additional details on crystal structure determination, magnetization measurements, resistivity measurements, heat capacity, upper critical fields and for additional band structure results and Fermi surfaces.

[24] H. Ku, Effect of composition on the superconductivity of the $E9_3$ phase in the ternary Nb-Rh-C system, Physica B+C **135**, 417 (1985).

[25] E. M. Carnicom, W. Xie, T. Klimczuk, J. Lin, K. Górnicka, Z. Sobczak, N. P. Ong, and R. J. Cava, $TaRh_2B_2$ and $NbRh_2B_2$: Superconductors with a chiral noncentrosymmetric crystal structure, Sci. Adv. **4**, eaar7969 (2018).

[26] M. Naito, A. Matsuda, K. Kitazawa, S. Kambe, I. Tanaka, and H. Kojima, Temperature dependence of anisotropic lower critical fields in $(La_{1-x}Sr_x)_2CuO_4$, Phys. Rev. B **41**, 4823 (1990).

[27] W. McMillan, Transition temperature of strong-coupled superconductors, Phys. Rev. **167**, 331 (1968).

[28] F. von Rohr, M. J. Winiarski, J. Tao, T. Klimczuk, and R. J. Cava, Effect of electron count and chemical complexity in the Ta-Nb-Hf-Zr-Ti high-entropy alloy superconductor, Proc. Natl. Acad. Sci. **113**, E7144 (2016).

[29] K. Górnicka, X. Gui, B. Wiendlocha, L. T. Nguyen, W. Xie, R. J. Cava, and T. Klimczuk, $NbIr_2B_2$ and $TaIr_2B_2$–New low symmetry noncentrosymmetric superconductors with strong spin–orbit coupling, Adv. Funct. Mater. **31**, 2007960 (2021).

[30] X. Gui and R. J. Cava, $LaIr_3Ga_2$: A superconductor based on a kagome lattice of Ir, Chem. Mater. **34**, 2824 (2022).

[31] L. Zeng, X. Hu, S. Guo, G. Lin, J. Song, K. Li, Y. He, Y. Huang, C. Zhang, P. Yu *et al.*, Ta_4CoSi: A tantalum-rich superconductor with a honeycomb network structure, Phys. Rev. B **106**, 134501 (2022).

[32] K. Stolze, J. Tao, F. O. von Rohr, T. Kong, and R. J. Cava, Sc-Zr-Nb-Rh-Pd and Sc-Zr-Nb-Ta-Rh-Pd high-entropy alloy superconductors on a CsCl-type lattice, Chem. Mater. **30**, 906 (2018).

[33] E. Helfand and N. Werthamer, Temperature and purity dependence of the superconducting critical field, H_{c2}. II, Phys. Rev. **147**, 288 (1966).

[34] T. Baumgartner, M. Eisterer, H. Weber, R. Flükiger, C. Scheuerlein, and L. Bottura, Effects of neutron irradiation on pinning force scaling in state-of-the-art Nb_3Sn wires, Supercond. Sci. Technol. **27**, 015005 (2014).

[35] L. C. Srivichitranond, E. M. Seibel, W. Xie, Z. Sobczak, T. Klimczuk, and R. J. Cava, Superconductivity in a new intermetallic structure type based on endohedral $Ta@Ir_7Ge_4$ clusters, Phys. Rev. B **95**, 174521 (2017).

[36] W.-H. Jiao, L.-P. He, Y. Liu, X.-F. Xu, Y.-K. Li, C.-H. Zhang, N. Zhou, Z.-A. Xu, S.-Y. Li, and G.-H. Cao, Superconductivity in $Ta_3Pd_3Te_{14}$ with quasi-one-dimensional $PdTe_2$ chains, Sci. Rep. **6**, 21628 (2016).

[37] C. Q. Xu, B. Li, J. J. Feng, W. Jiao, Y. K. Li, S. W. Liu, Y. X. Zhou, R. Sankar, N. D. Zhigadlo, H. B. Wang *et al.*, Two-gap superconductivity and topological surface states in TaOsSi, Phys. Rev. B **100**, 134503 (2019).

[38] Z. Shi, S. J. Kuhn, F. Flicker, T. Helm, J. Lee, W. Steinhardt, S. Dissanayake, D. Graf, J. Ruff, G. Fabbris *et al.*, Incommensurate two-dimensional checkerboard charge density wave in the low-dimensional superconductor $Ta_4Pd_3Te_{16}$, Phys. Rev. Res. **2**, 042042(R) (2020).

[39] T. Shang, J. Z. Zhao, D. J. Gawryluk, M. Shi, M. Medarde, E. Pomjakushina, and T. Shiroka, Superconductivity and topological aspects of the rocksalt carbides NbC and TaC, Phys. Rev. B **101**, 214518 (2020).

[40] T. Klimczuk, S. Królak, and R. J. Cava, Superconductivity of Ta-Hf and Ta-Zr alloys: Potential alloys for use in superconducting devices, Phys. Rev. Mater. **7**, 064802 (2023).

[41] J. A. T. Barker, B. D. Breen, R. Hanson, A. D. Hillier, M. R. Lees, G. Balakrishnan, D. M. Paul, and R. P. Singh, Superconducting and normal-state properties of the noncentrosymmetric superconductor Re_3Ta, Phys. Rev. B **98**, 104506 (2018).

[42] X. Gui, K. Górnicka, Q. Chen, H. Zhou, T. Klimczuk, and W. Xie, Superconductivity in metal-rich chalcogenide Ta_2Se, Inorg. Chem. **59**, 5798 (2020).

[43] Y. Lu, T. Takayama, A. F. Bangura, Y. Katsura, D. Hashizume, and H. Takagi, Superconductivity at 6 K and the violation of Pauli limit in $Ta_2Pd_xS_5$, J. Phys. Soc. Jpn. **83**, 023702 (2014).

[44] L. Yan, C. Ding, M. Li, R. Tang, W. Chen, B. Liu, K. Bu, T. Huang, D. Dai, X. Jin *et al.*, Modulating charge-density wave order and superconductivity from two alternative stacked monolayers in a bulk 4Hb-$TaSe_2$ heterostructure via pressure, Nano Lett. **23**, 2121 (2023).

[45] H. X. Liu, J. Y. Yao, J. M. Shi, Z. L. Yang, D. Y. Yan, Y. Li, D. H. Chen, H. L. Feng, S. L. Li, Z. J. Wang *et al.*, Vanadium-based superconductivity in the breathing kagome compound $Ta_2V_{3.1}Si_{0.9}$, Phys. Rev. B **108**, 104504 (2023).

[46] T. Terashima, Y. Tokumoto, K. Hamano, T. Konoike, N. Kikugawa, and K. Edagawa, Anomalous upper critical field in the quasicrystal superconductor $Ta_{1.6}Te$, npj Quantum Mater. **9**, 56 (2024).

[47] K. Ma, J. Lago, and F. O. von Rohr, Superconductivity in the η-carbide-type oxides $Zr_4Rh_2O_x$, J. Alloys Compd. **796**, 287 (2019).